AIAA JOURNAL
Vol. 40, No. 10, October 2002

Flow Control of Circular Cylinders with Longitudinal Grooved Surfaces

Hee-Chang Lim* and Sang-Joon Lee†
Pohang University of Science and Technology, Pohang 790-784, Republic of Korea

Flow around circular cylinders with different grooved surfaces (U and V shaped) was investigated experimentally. The drag force, mean velocity, and turbulence intensity profiles of the wake behind the cylinders were measured for Reynolds numbers based on the cylinder diameter ($D = 60$ mm) in the range $Re_D = 8 \times 10^3 \sim 1.4 \times 10^5$. Flow around the cylinders was visualized using a particle tracer technique to see the flow structure qualitatively. The results were compared with those for a smooth cylinder of the same diameter D. At $Re_D = 1.4 \times 10^5$, the U-type groove surface reduced the drag coefficient by 18.6% compared with the smooth cylinder, whereas the drag reduction of V-type grooves was only 2.5%. For the circular cylinder with a U-grooved surface, as the Reynolds number increases, the location of peak turbulence intensity moves downstream, and the turbulence intensity is decreased. The two longitudinal-grooved surfaces tested in this study show different surface pressure distributions at high Reynolds numbers due to their different flow structures near the cylinder surface. Flow visualization results show that the U-grooved cylinder elongates the vortex formation region more than 50% compared with the smooth cylinder. This is consistent with the results of turbulence intensity distribution measured along the wake centerline. The large-scale longitudinal vortices formed behind the grooved cylinders seem to be broken into smaller ones due to the existence of longitudinal grooves. On average, the scale of longitudinal vortices behind the U-grooved cylinder is much smaller in size compared with the other two cases.

Nomenclature

C_D	=	drag coefficient
C'_D	=	pressure drag coefficient
C_p	=	pressure coefficient $(p - p_0)/(0.5\rho U_0)$
D	=	diameter of cylinder
f_0	=	dominant shedding frequency
h	=	height of the grooves
L	=	length of cylinder
p	=	static pressure
p_0	=	freestream static pressure
Re_c	=	critical Reynolds number, 3×10^5
Re_D	=	Reynolds number, $U_0 D/\nu$
$S(f)$	=	spectral density function
Sr	=	Strouhal number, fD/U_0
S_u	=	standard deviation
s	=	spacing between adjacent grooves
U_0	=	freestream velocity
θ	=	angle from the stagnation point
ν	=	kinematic viscosity

Introduction

DURING the past few decades, the control of wakes behind bluff bodies has been important theme in many engineering applications. In particular, recent advanced technologies such as microfabrication and active feedback control make it possible to employ artificial manipulations on drag force. Because drag reduction is closely related with energy saving, extensive effort has been made over recent decades to reduce the drag acting on moving vehicles.

There are two types of flow control techniques, active and passive. Active control methods require a certain energy input, for example, to suck or blow some of the flow to delay transition, to modify the fluid viscosity with polymers, or to change the fluid temperature. Passive control, however, does not require any auxiliary power input, only a change in surface configuration or attachment to the main body of additive devices such as riblets or large-eddy breakup devices.[1] Passive control methods are cost effective because they require no additional energy input, provided the main body is streamlined and optimized in shape. Bandyopadhyay[2] reviewed various drag reduction techniques and surface modification. He investigated mean flow over longitudinal-grooved surfaces and outer-layer devices. In addition, many researchers have studied the effects of surface modifications on turbulent boundary layers.[3–6] Also the formation and evolution of vortices from a circular cylinder have been widely investigated with great interest. Williamson[7] reviewed the vortex dynamics in the cylinder wake.

There are several aerodynamic means for controlling vortex structure around a cylinder. Zdravkovich[8] reviewed the methods of suppressing vortices shed from a cylinder. He reported that the main governing factor for high effectiveness is the vortex formation length. However, he did not reveal the large-scale coherent structure changed by the suppressing methods. Among effective flow control methods, the surface protrusions modify the wake structure by changing separation lines and/or surface flow directions.

Using surface protrusions, Weaver[9] controlled the flow-induced vibrations of the circular members of large radar antenna frames. He obtained an empirical curve for the lift coefficients in terms of Reynolds number and found that the most effective pitch was $12D$ with four helical windings whose diameter was $0.094D$. Nebres and Batill[10] investigated flow characteristics around slender bluff bodies having helical surface protrusions. They measured time-averaged wake velocity profiles behind two different models using a single hot-wire probe, yawed stranded cables and cylinders wrapped with four small helical wires. Lee and Kim[11] investigated the flow characteristics of the controlled wake behind a circular cylinder ($D = 40$ mm) wrapped helically by three small wires ($d = 0.075D$) with pitches of $5D$ and $10D$. They found that the surface protrusions elongate the vortex formation region, decrease the vortex shedding frequency, and shrink the wake width.

Most previous studies have investigated the flow structure over riblet surfaces placed on a flat plate. Walsh[3] investigated drag reduction of longitudinal ribs of rectangular, triangular, and transversely curved shapes. He reported that the drag reduction was associated with a decrease of momentum thickness and turbulent velocity fluctuations and depended mainly on the riblet configuration such as

Received 19 July 2001; revision received 29 December 2001; accepted for publication 27 May 2002.

*Ph.D. Student, School of Environmental Science and Engineering, San 31 Hyoja-Dong.

†Professor, Department of Mechanical Engineering, San 31 Hyoja-Dong; sjlee@postech.ac.kr.

the height h, spacing s, and shape. He suggested that a riblet with sharp peaks and large valley curvature is one of the optimum riblet shapes for drag reduction. Lee and Lee[12] investigated the flow structure over a semicircular riblet surface. They measured the near-wall turbulent structures over semicircular (U-type) grooves of $s = 3$ mm using particle image velocimetry (PIV) velocity field measurement technique and found how the semicircular riblet reduces the drag acting on the surface. As an extension of this study to a bluff body, we tested the U- and V-grooved cylinders having the same groove spacing of $s = 3$ mm in the present study.

The longitudinal grooves have been revealed as an effective flow control technique for drag reduction and heat transfer enhancement.[1] The performance depends largely on the configuration of the adapted groove surfaces. In applications of riblet surfaces on bluff bodies, Achenbach[13] and Guven et al.[14] found that the surface roughness on a circular cylinder affected the vortex shedding, the drag coefficient, and the heat transfer characteristics. Ko et al.[15] and Leung and Ko[16] measured the mean pressure distributions and Strouhal number variation for V-grooved circular cylinders in the Reynolds number range $2 \times 10^4 \sim 1.6 \times 10^5$. In their study, the V-groove and smooth cylinders had almost the same drag coefficient. They focused on the effect of different groove configurations on the reduction of drag acting on the cylinder.

Although the flow control for drag reduction is very important in engineering applications and has attracted much attention, the controlled wake structure behind a bluff body with grooved surfaces has not been fully understood. In addition, there are still some contradictions about the mechanism by which longitudinal grooves reduce the drag acting on bluff bodies with grooved surfaces. From an aerodynamic point of view, it is also important to know the wake structure modified by the grooved surface and to understand the vortex suppressing process in the near wake. Therefore, in this study, we focused our attention to the modification of the wake structure of a circular cylinder having longitudinal V and U grooves. We measured surface pressure, drag force, and wake velocity and visualized the flow structure. The main objective of this study is to investigate experimentally the effect of the groove configuration (U and V shaped) on drag reduction and on the variation of flow structure in the near wake.

Experimental Apparatus and Method

Wind Tunnel and Experimental Model

Experiments were performed in a closed-return-type subsonic wind tunnel with a test section of 0.72-m width, 0.6-m height, and 6-m length. The freestream turbulence intensity in the test section was less than 0.08% at $U_0 = 10$ m/s. This level of freestream turbulence is sufficient for the proposed study on the wake structure behind bluff bodies.[17] The flow characteristics around the cylinders were measured with varying the Reynolds number (based on the cylinder diameter D) in the range $Re_D = 8 \times 10^3 \sim 1.4 \times 10^5$.

Three circular cylinders of the same outer diameter ($D = 60$ mm) with different surface configurations were tested. One cylinder had a smooth surface. The other two cylinders had longitudinal grooves, one with a saw-toothed (V-grooved) shape, the other cylinder with a semicircle (U-grooved) shape. The experimental models were made of Teflon® pipe of length $L = 600$ mm. Graham[18] reported that the vortex shedding process was quite different from that occurring on an infinitely long cylinder when the aspect ratio L/D was smaller than 3.8. In this respect, the cylinders of $L/D = 10$ tested in this study can be considered roughly as a two-dimensional cylinder. The configuration and the coordinate system of the grooved cylinders tested in this study are shown in Fig. 1. Lee and Lee[12] investigated the flow structure over a U-shaped grooved plate using PIV velocity field measurement technique. They investigated the near-wall flow structure inside the semicircular grooves of $s = 3$ mm. Walsh[3] suggested that the semicircular riblet with sharp peaks is one of the optimum groove shapes for drag reduction. In present study, we used the U- and V-grooved cylinders having the same groove spacing of $s = 3$ mm. For a systematic analysis, the two different kinds of grooved cylinders are required to have the same sizes of s and h. From a practical viewpoint of the manufacturing process, however, it was nearly impossible. In addition, the groove spacing(s) has been known more important, compared with the groove height h. Therefore, we focused our attention on the peak shape (U and V) of grooves having the same lateral spacing s.

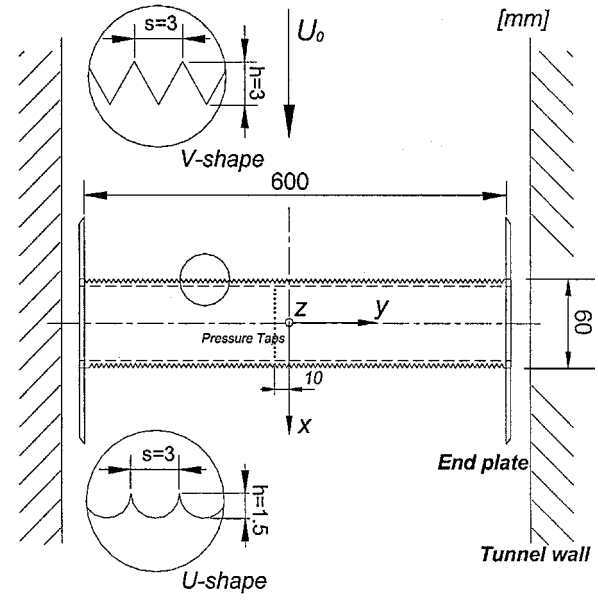

Fig. 1 Schematic of test cylinders and coordinate system.

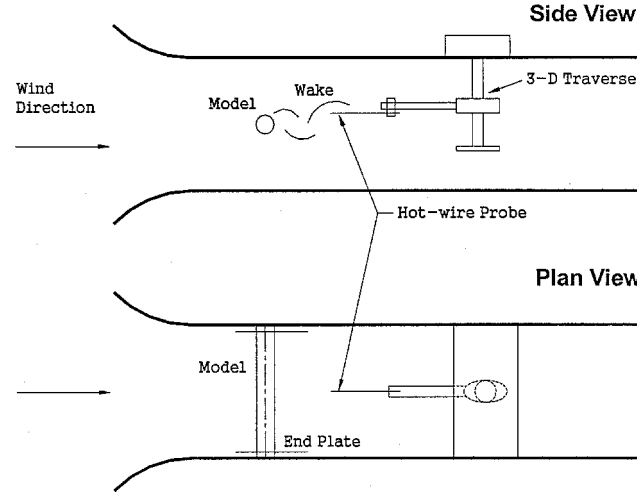

Fig. 2 Wind-tunnel test section and experimental setup.

The cylinder models were installed horizontally 260 mm above the bottom surface in the central region of the wind-tunnel test section. A schematic diagram of the experimental setup is given in Fig. 2. In the considerations of groove fabrication and higher Reynolds number, a little larger cylinder was used in this study. With the installation of a cylinder of diameter $D = 60$ mm, the blockage ratio was about 8%. To correct for the blockage ratio and wall interference effects, we employed the formulas of Allen and Vincenti[19] to correct the values of velocity, pressure, and drag coefficient. Two square end plates, 300×300 mm with a 2-mm thickness, were used to minimize the effect of a boundary layer developing along the tunnel sidewalls and to maintain two-dimensional flow characteristics in the cylinder wake. The shape and size of the plates were determined following the results of Stansby.[20]

Flow Measurements

Figure 3 shows the schematic diagram of the drag, velocity, and surface pressure measurement system. For the measurement of drag force acting on the cylinder, two combined sets of a dummy cylinder and a load cell were attached on the tunnel wall. To avoid the tunnel wall interference acting on the cylinder, concentric dummy cylinders about 5 cm long and end plates were installed at both sides of the

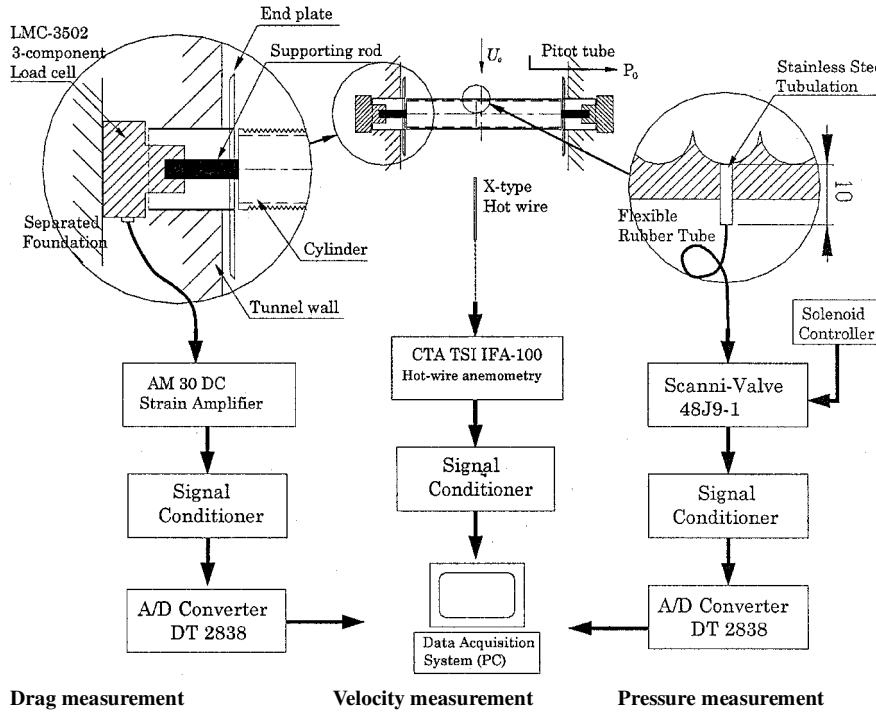

Fig. 3 Schematic of drag, velocity, and pressure measurement system.

wind-tunnel test cylinder. The aerodynamic forces were measured using two three-component load cells (Nissho LMC-3502) whose rated load is ±5 kg and nonlinearity is within ±0.5%. The test cylinders were supported at both sides using the same load cells: one for measuring forces and the other for dummy balancing. The load cell was coupled to a high-gain dc strain amplifier (DSA-100) and connected to a personal computer through a DT2838 A/D converter.

The drag coefficient based on the effective frontal area of the cylinder A was defined as follows:

$$C_D = \frac{2 \times \text{drag}}{\rho U_0^2 A} \tag{1}$$

Wake velocity profiles were measured using I-type (DANTEC 55P11) and X-type hot-wire probes (DANTEC 55P61) connected to a constant temperature hot-wire anemometer (TSI IFA 100) and DT2838 A/D converter. The hot-wire probe was traversed to the measuring positions using a three-dimensional traverse system with an accuracy of 0.01 mm. At each measurement point, 32,768 velocity data were acquired at 2000 samples/s after low-pass filtering at 800 Hz. During the experiments, the temperature variation in the wind-tunnel test section was maintained to be less than 0.5°C. The vertical mean velocity and turbulence intensity profiles were measured in the range $z/D = -3 \sim 3$ at $0.1D$ intervals at the downstream sections of $x/D = 4$ and 6. To investigate the vortex structure of the near wake behind the cylinder, the dominant shedding frequency of velocity signals from an I-type hot-wire probe located at $x/D = 2$, $y/D = 0.5$ was spectrally analyzed.

To measure surface pressure distributions, 36 taps were installed flush with the bottom of the grooves along the longitudinal axis of the cylinder at a 10-mm interval from the midsection of the wind tunnel (Figs. 1 and 3). Pressure distributions were measured by rotating the cylinder in 10-deg increments. The inner diameter of the stainless steel pressure taps was 0.8 mm. The pressure taps were connected to a micromanometer (FCO-19), and the analog pressure signals were digitized using a high-precision A/D converter (DT-2838). At each measurement point, 16,384 pressure data were acquired at a 500-Hz sampling rate after low-pass filtering at 200 Hz. A time delay of a few seconds was given to recover pressure fluctuations after each channel scanning.

The pressure difference between the surface pressure p on the cylinder surface and the static pressure p_0 measured at the location of $x/D = -8$, $y/D = 3$, and $z/D = 2$. The pressure difference was nondimensionalized by the dynamic pressure $0.5\rho U_0^2$ to give the pressure coefficient C_p in the following form:

$$C_p = \frac{(p - p_0)}{0.5\rho U_0^2} \tag{2}$$

In addition, the surface pressure data were integrated to give the pressure drag coefficient C_D'.

Flow Visualization in the Water Channel

A particle tracer technique was employed to visualize the qualitative flow pattern in the wake behind the cylinder. Polyvinylchloride particles with an average diameter of 300 μm were seeded as tracer particles in a circulating water channel with a test section of 0.3 (width) × 0.25 (height) × 1.2 (length) m^3. The particle streaks were illuminated with a thin, cold light sheet, emitted from a 150-W halogen lamp (NPI PICL-NEX). The scattered particle images at a freestream velocity of 20 cm/s ($Re_D = 1.25 \times 10^4$) were photographed with a Nikon F5 camera. Because of the limited physical size of the water channel, the blockage ratio of the cylinder model was about 25% in this flow visualization experiment, higher than that (8%) used for the wind-tunnel tests. From a practical point of view, however, our attentions were focused on the variation in wake structure behind the cylinders qualitatively.

It is difficult to interpret and analyze three-dimensional unsteady flow patterns conceptually. Perry and Chong[21] reported that the topological description of flow patterns using critical-point concepts could provide a framework and methodology for overcoming this kind of difficulty. In their theory, by the classification of critical points into several topological terms such as nodes, saddles, and foci, the topologically correct pattern of limiting streamlines can be recognized immediately. In this study, the critical-point theory was applied to identify the instantaneous topological features of the near wake behind the cylinders.

Uncertainty Analysis

All experimental data may contain more or less uncertainty. The uncertainty analysis was carried out for all experimental results to assess the confidence level, following the method suggested by Coleman.[22] The total error consists of bias error and precision error. The bias error can be minimized with careful calibration of measuring instruments.

To evaluate the precision error, the standard deviation S_u of five sample records was calculated for the velocity, pressure, and force data measured for each cylinder. The value of the t-distribution for 95% confidence and five samples was 2.776. The total error with 95% confidence was depicted as a form of error bar.

Results and Discussion

Drag Force

Figure 4 shows the variation in drag coefficient with varying Reynolds number. The drag coefficients were corrected in consideration of the blockage effect by applying the method suggested by Allen and Vincenti.[19] For comparison, the results of Ko et al.[15] and Wieselsberger[23] are included. The pressure drag coefficient C'_D obtained by integrating the pressure data around the cylinder surface is also included in Fig. 4. Error bars indicate the error encountered in obtaining the mean values with 95% confidence level.

The drag coefficient for the smooth cylinder model agrees well with those of previous results measured in the ranges of $10^4 < Re_D < 10^5$. The drag coefficient of the smooth circular cylinder is nearly constant and has an average value of 1.2. In addition, the pressure drag coefficient C'_D is nearly well matched with total drag coefficients within the subcritical regime. From this, we can conjecture that the pressure drag coefficient for the grooved cylinders shows a similar tendency in the same range of Reynolds numbers.

The drag coefficients of the grooved cylinders show a similar tendency to the smooth cylinder up to a Reynolds number of 4×10^4. Thereafter, the drag coefficient of the cylinder with U grooves decreased substantially. Ko et al.[15] found similar behavior for a V-grooved cylinder in the Reynolds number range from 2×10^4 to 1.6×10^5. He reported that the transitions from subcritical to critical and from critical to supercritical flow regimes for the V-grooved cylinder occur at lower Reynolds numbers than for the smooth cylinder. In our study, the flow regime does not reach the critical Reynolds number; however, the drag coefficients for the smooth and V-grooved cylinders show a similar trend with respect to Reynolds number.

Even though the general trend is similar, the Ko et al.[15] result for the grooved cylinder has much smaller C_D values at high Reynolds numbers. The large difference in C_D values for the V-grooved cylinder seems to be caused by the different geometric shape of longitudinal grooves and different experimental conditions. They measured pressure distribution on the cylinder surface, whose height was relatively small, to calculate their drag coefficients. The maximum groove height was 1.22 mm, immersed in a turbulent boundary layer developed on the cylinder surface. Therefore, in addition to the pressure drag, the contribution of friction drag due to riblet effect should be considered in the total drag calculation. In addition, Ko et al.[15] used an equivalent diameter d_{eq} for the V-grooved cylinder, taking into account the surface area increase caused by grooves. For the U-grooved cylinder at $Re_D = 1.83 \times 10^4$, the difference between the total drag and pressure drag coefficient is about $2 \sim 3\%$.

The V-grooved cylinder shows drag reduction of about 2.5% at $Re_D = 1.4 \times 10^5$ compared with that of the smooth circular cylinder in the subcritical regime. The drag coefficient of the U-grooved circular cylinder, however, is reduced by 18.6% at $Re_D = 1.4 \times 10^5$.

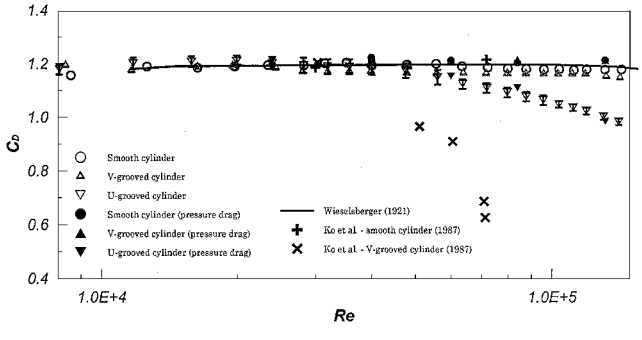

Fig. 4 Variation of drag coefficient with Reynolds number.

Flow Characteristics

Figures 5 and 6 show vertical profiles of the streamwise mean velocity and turbulence intensity measured at downstream locations of $x/D = 4$ and 6 for two Reynolds numbers, $Re_D = 4 \times 10^4$ ($U_0 = 10$ m/s) and 8×10^4 ($U_0 = 20$ m/s). The uncertainty encountered on the mean velocity U/U_0 was less than 1.3%. The mean streamwise velocity profiles show a large velocity deficit in the wake region. The wake width at $x/D = 6$ is about 13% wider than that at $x/D = 4$. At $U_0 = 10$ m/s ($Re_D = 4 \times 10^4$), the mean velocity and turbulence intensity of the streamwise velocity measured at $x/D = 4$ and 6 show little difference between the smooth cylinder and the U-grooved cylinder.

Figure 6 shows the streamwise mean velocity and turbulence intensity profiles at $U_0 = 20$ m/s. As the Reynolds number increases, the flow structure shows a slightly larger difference between the smooth and U-grooved cylinders, compared with that at $U_0 = 10$ m/s. In addition, the turbulence intensity profiles have more distinct double peaks and larger values than those at $U_0 = 10$ m/s. At $U_0 = 10$ m/s ($Re_D = 4 \times 10^4$), the grooved cylinder has nearly the same wake (half) width as the smooth cylinder. However, at higher Reynolds number $Re_D = 8 \times 10^4$, the U-grooved cylinder has smaller wake width, compared with the smooth cylinder. The reduction of wake width at the downstream location of $x/D = 6$ is about 6.4%.

To estimate the drag coefficient in another way, the momentum deficit at $x/D = 4$ was investigated from the streamwise mean velocity profiles using the momentum-integral theory.[24] As a result, the smooth cylinder has drag coefficient of $C_D = 1.17$ at $U_0 = 10$ m/s ($Re_D = 4 \times 10^4$). At higher velocity of $U_0 = 20$ m/s

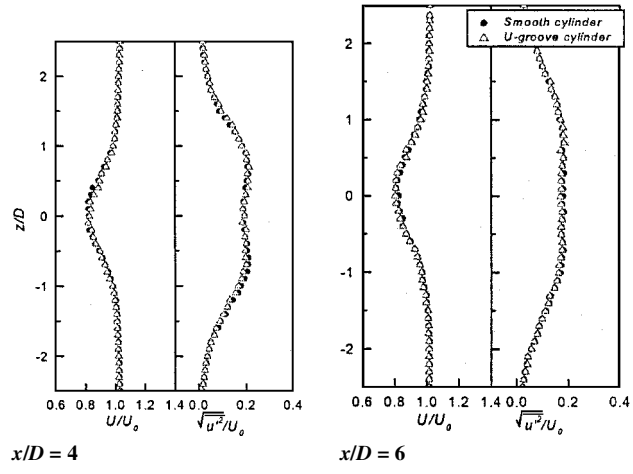

Fig. 5 Streamwise mean velocity and turbulent intensity profiles at $U_0 = 10$ m/s; uncertainty in $U/U_0 < \pm 1.3\%$.

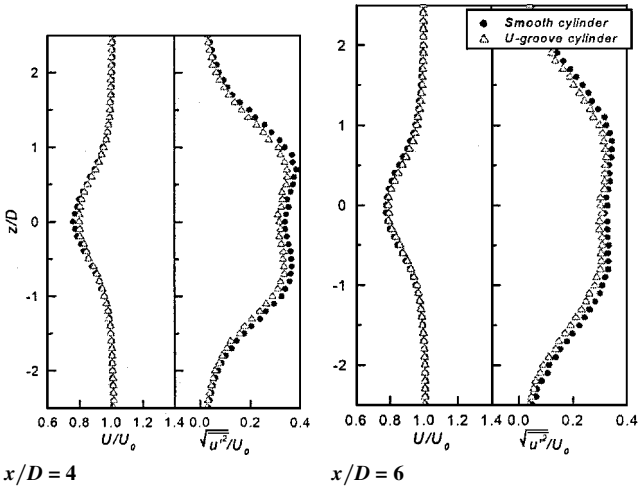

Fig. 6 Streamwise mean velocity and turbulent intensity profiles at $U_0 = 20$ m/s; uncertainty in $U/U_0 < \pm 1.3\%$.

($Re_D = 8 \times 10^4$), however, the U-grooved cylinder has $C_D = 1.07$, an 8.5% drag reduction from that of smooth cylinder. These results are in good agreement with the total drag variation shown in Fig. 4.

The U-grooved cylinder has smaller deficit of mean velocity and lower turbulent fluctuations in the near-wake region in comparison with the smooth cylinder. From this, we can conjecture that the total drag of the U-grooved cylinder is smaller than that of the smooth cylinder.

Vortex Formation Region

Bloor[25] defined the end of the formation region as the point after which oscillating wake characteristics are observed. This implies that vortices shed from both sides of the cylinder cross the wake axis at the end of the formation region.

Figure 7 shows the turbulence intensity distribution of the streamwise velocity component measured along the wake centerline at 5-mm intervals. Measurements were performed for three cylinders (smooth, V groove, and U groove) in the Reynolds number range $Re_D = 1.6 \times 10^4 \sim 1.0 \times 10^5$. The velocity signals were bandpass filtered at the vortex shedding frequency and measured using an I-type hot-wire probe. For a smooth cylinder, as the flow goes downstream, the streamwise turbulence intensity increases initially and reaches a peak value at approximately $x/D = 1$; thereafter, it begins to decrease.

The peak streamwise turbulence intensity for the smooth cylinder moves toward the cylinder as the Reynolds number increases. The cylinder with V grooves has a peak value slightly downstream of the smooth cylinder, depending on Reynolds number. However, the turbulence intensity distribution for the V-grooved cylinder is almost the same as that of the smooth circular cylinder, excluding in the region $x/D = 0 \sim 1$ just behind the cylinder. On the other hand, the peak for the U-grooved cylinder shifts downstream as the Reynolds number increases. In addition, the magnitude of the turbulence intensity in the wake region decreases with increasing Reynolds number, especially in the near wake region $x/D = 0 \sim 2$. From these results, it can be conjectured that the U-grooved surface reduces velocity fluctuations in the wake region and elongates the vortex formation region in the downstream direction.

In the present study, the end of the formation region was defined as the peak in the turbulence intensity distribution. Streamwise turbulence intensity data measured along the wake centerline were curve fitted using a fifth-order polynomial to find the peak location for each

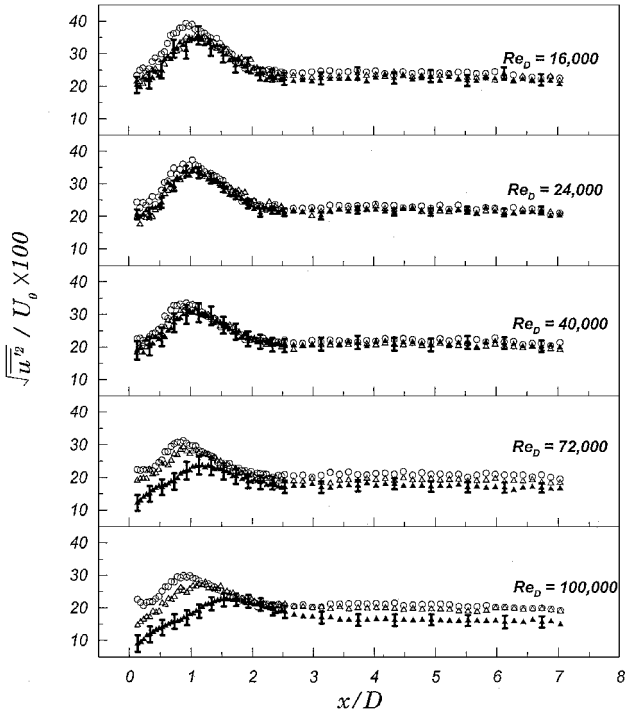

Fig. 7 Turbulence intensity distributions along the wake centerline: ○, smooth; △, V groove; and ▲, U groove.

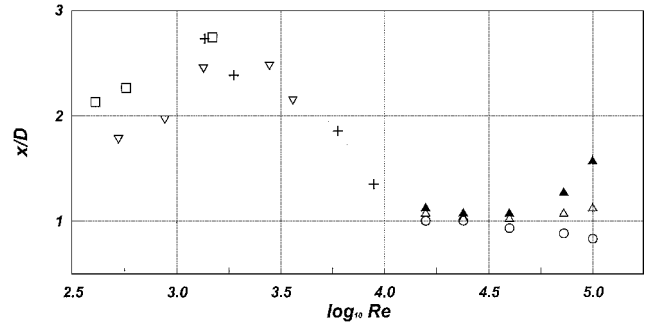

Fig. 8 Lengths of formation region: ○, smooth; △, V groove; ▲, U groove; and Bloor[25]: +, d = 6.4; ▽, d = 3.2; and □, d = 2.5 mm.

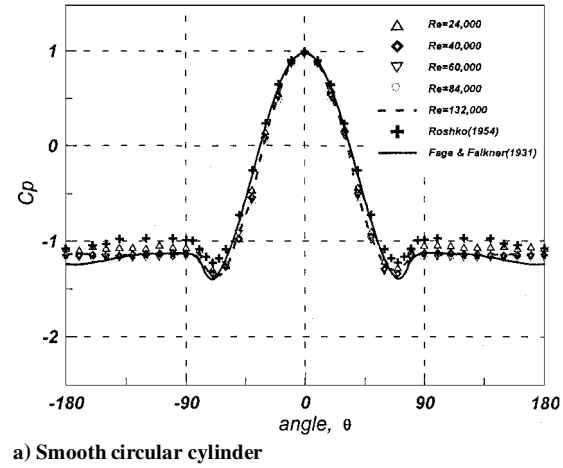

a) Smooth circular cylinder

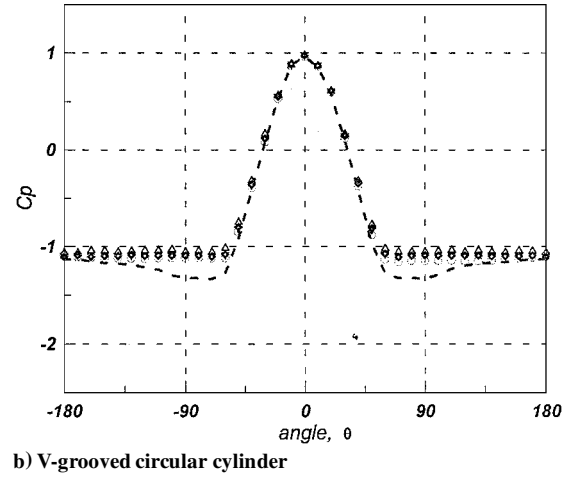

b) V-grooved circular cylinder

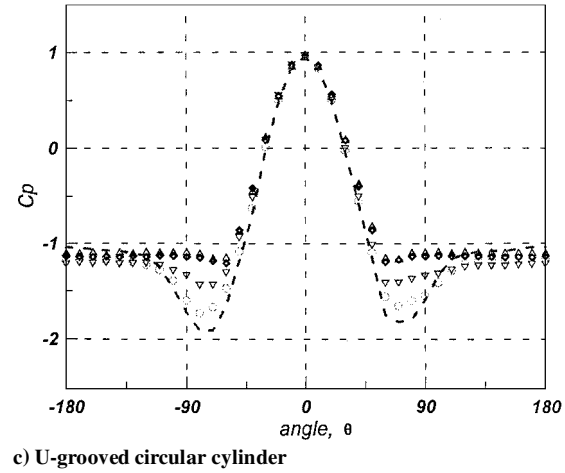

c) U-grooved circular cylinder

Fig. 9 Comparison of surface pressure distributions; uncertainty in $C_p < \pm 2\%$.

Reynolds number. The lengths of the formation region determined from the fitted peak values are shown in Fig. 8. For comparison, the results of Bloor[25] are also included. Bloor reported that the length of the formation region increases to 2.5 diameters before steadily decreasing with increasing Reynolds number.

For the smooth cylinder tested in this study, the length of the vortex formation region decreased linearly with increasing Reynolds number. On the other hand, the length of the vortex formation region of the grooved cylinders tends to increase rapidly. In particular, the rate of length increase for the U-grooved cylinder with respect to Reynolds number is larger than that of V-grooved cylinder, as shown in Fig. 8.

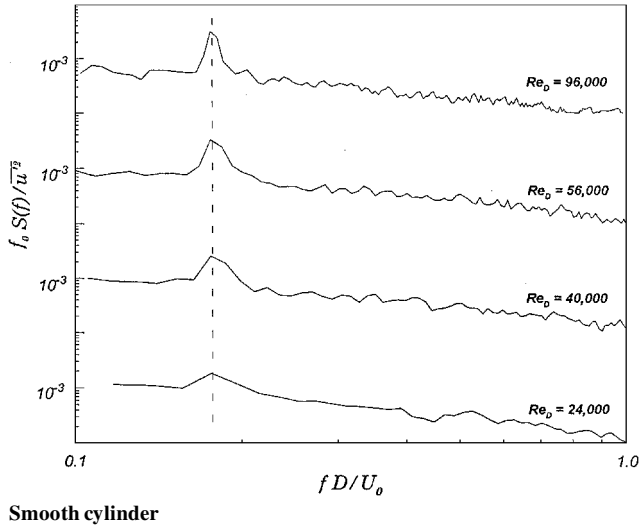

Smooth cylinder

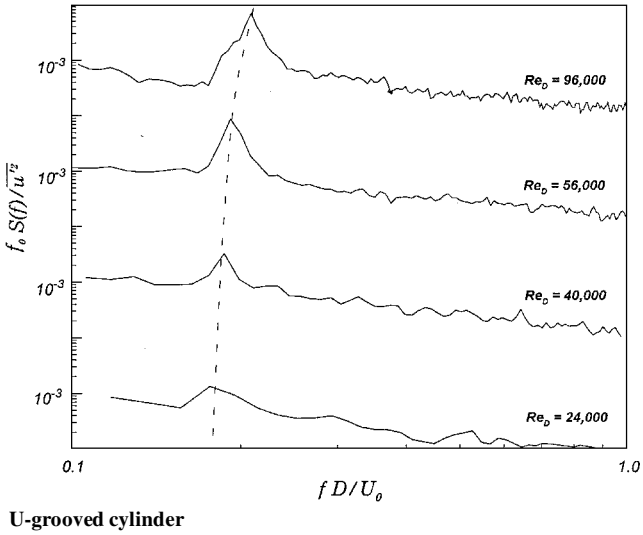

U-grooved cylinder

Fig. 10 Comparison of nondimensional PSD distribution.

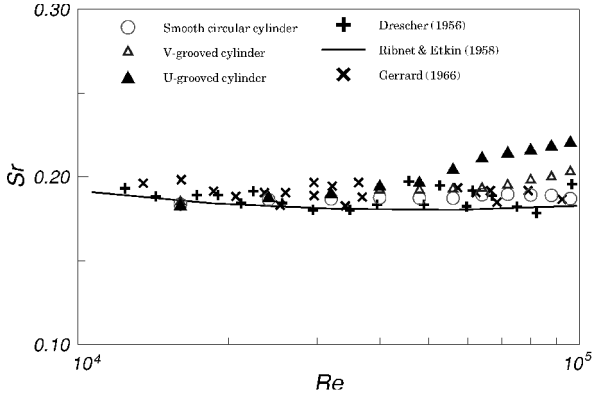

Fig. 11 Strouhal number variation with Reynolds number.

Surface Pressure

The effect of Reynolds number on the pressure distribution measured at the midsection of three cylinders is shown in Fig. 9. For comparison, the results of Roshko,[26] at $Re = 1.45 \times 10^4$ and Fage and Falkner[27] at $Re = 1.1 \times 10^5$ for a smooth cylinder were included.

In the subcritical regime, less than the critical Reynolds number $Re_c = 3 \times 10^5$, the boundary layer separated in a laminar state at about 80 deg from the forward stagnation point, and the early separation causes a drag coefficient of about 1.2. The pressure

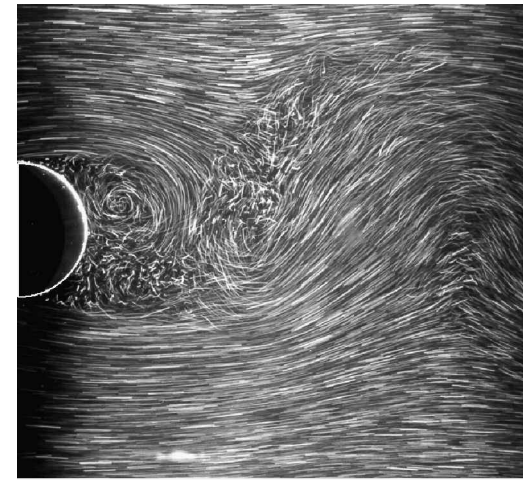

Smooth circular cylinder

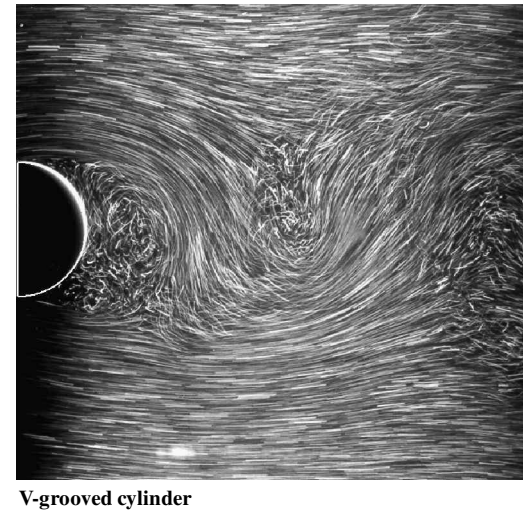

V-grooved cylinder

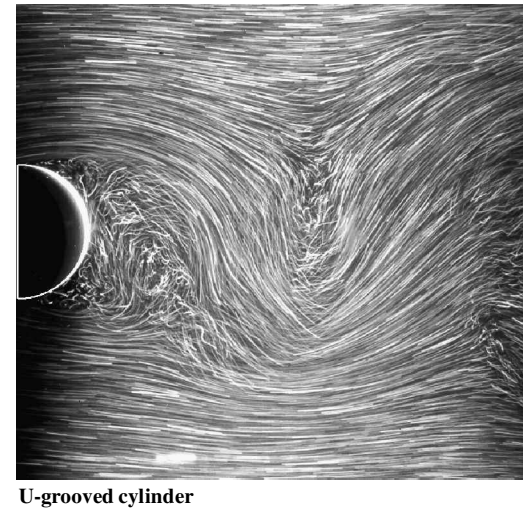

U-grooved cylinder

Fig. 12 Visualized flow using a particle tracer method in streamwise vertical plane.

coefficient of the smooth cylinder agrees well with those of Roshko[26] and Fage and Falkner.[27] For the smooth cylinder, the surface pressure distribution does not show remarkable variation in the range of $2 \times 10^4 < Re_D < 1.3 \times 10^5$.

Even though the flow belongs to the subcritical regime, the pressure distributions on the V- and U-grooved cylinders are quite different from that on a smooth cylinder. For the V-grooved cylinder (Fig. 9b), the mean pressures on the cylinder surface in the region behind the separation point have nearly constant values, except for the high Reynolds number of $Re_D = 1.32 \times 10^5$. The pressure drag coefficients C'_D shown in Fig. 4 are obtained by integrating these surface pressure distributions on the smooth and grooved cylinders.

The pressure distributions of the U-grooved cylinder (Fig. 9c) are quite different from those of the smooth and V-grooved cylinders, even though the flow is within the subcritical regime. The surface pressure distribution has large variations around the separation region over the cylinder. As the Reynolds number increases, the separation point shifts downstream, and the surface pressure decreases. This may be attributed the longitudinal grooves on the cylinder surface enhancing the boundary layer transition from laminar to turbulent flow. In addition, the base pressure at Reynolds number $Re_D = 1.32 \times 10^5$ is higher than that at Reynolds number $Re_D = 2.4 \times 10^4$. From these results, it can be conjectured that the U-grooved surface causes a substantial decrease in the drag at high Reynolds numbers, compared with the other two cylinders.

Spectral Analysis

The power spectral density (PSD) distributions measured at a downstream location $x/D = 2$, $y/D = 0.5$ are shown in Fig. 10 for four Reynolds numbers: $Re_D = 2.4 \times 10^4$, 4×10^4, 5.6×10^4,

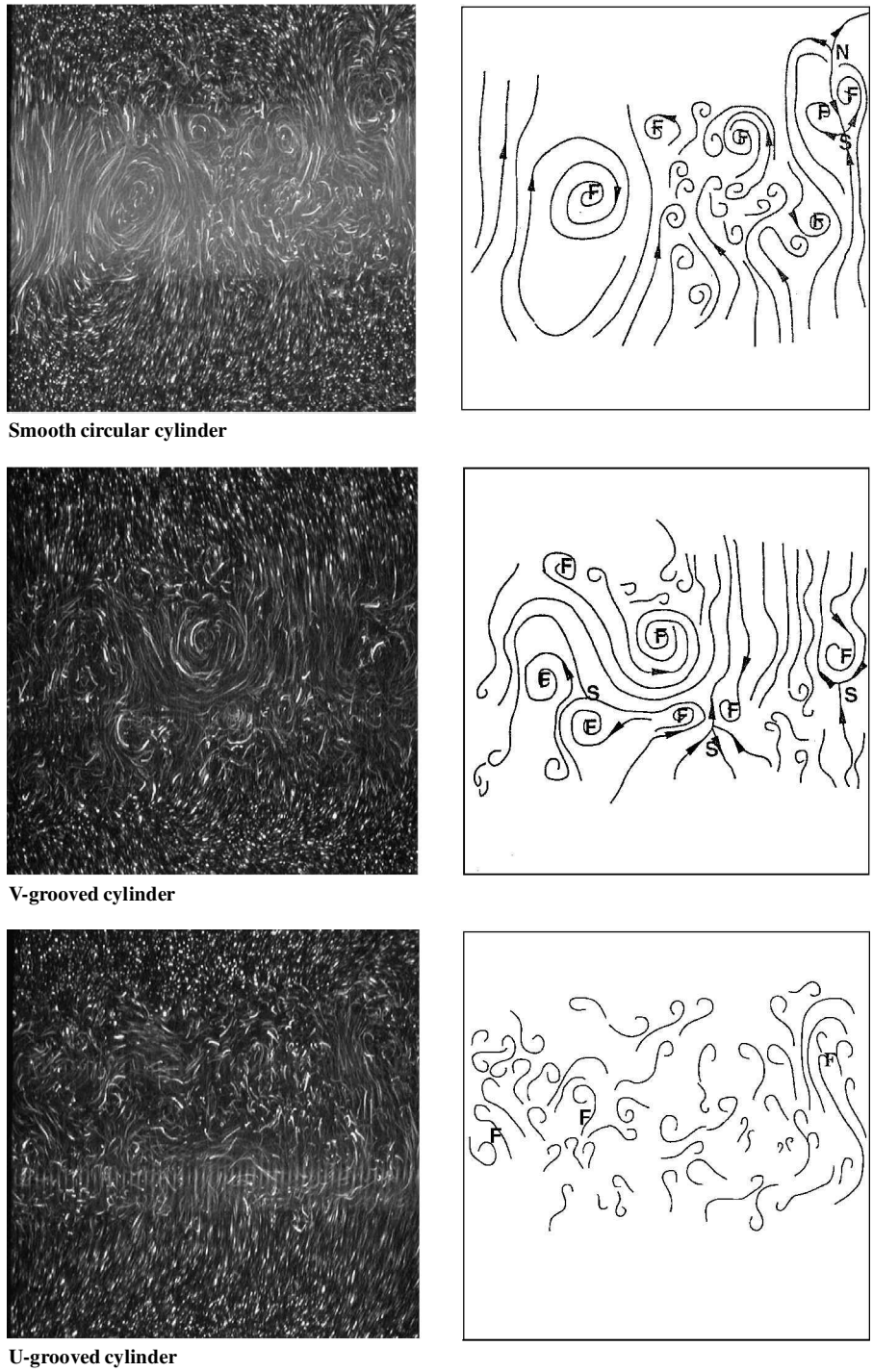

Fig. 13 Visualized flow in spanwise vertical cross-section at $x/D = 1.0$: F, focus; N, node; S, saddle with left the visualized flow and right the interpretation of flow pattern.

and 9.6×10^4. The vortex shedding frequency f is represented in a nondimensional parameter, the Strouhal number $Sr = fD/U_0$. In Fig. 10, $S(f)$ and f_0 in the y axis are the PSD function and the dominant shedding frequency, respectively. Here, a clear and distinct peak indicates the existence of a dominant vortex structure due to regular vortex shedding. In Fig. 10, the dotted line represents the peak location, indicating vortex shedding frequency.

As the Reynolds number increases, the peak become distinctive and the Strouhal number corresponding to peak location approaches a value of $fD/U_0 = 0.185$. However, for the case of the U-grooved cylinder, the vortex shedding frequency increases with the increase of Reynolds number.

Figure 11 shows the variation of Strouhal number with respect to Reynolds number. The experimental results of previous studies[28–30] for a circular cylinder are compared in Fig. 11. The Strouhal number for the smooth cylinder agrees well with others. In addition, the Strouhal number for the smooth circular cylinder has an almost constant value of around $0.18 \sim 0.195$. On the other hand, the Strouhal numbers for grooved cylinders increase gradually with increasing Reynolds number. The increase of the Strouhal number for the U-grooved cylinder at higher Reynolds number is remarkable compared with the V-grooved cylinder. These results indicate that U grooves on the cylinder surface effectively suppress vortices formed behind the cylinder and elongate the vortex formation region, enhancing vortex shedding from the cylinder.

Flow Visualization

The wakes behind the three types of cylinders were visualized using the particle tracer method to see the flow structure, especially the vortex structure in the near wake region. Wei and Smith[31] mentioned the generation of secondary vortices as the degree of complexity of free-shear layer, which is distinctly different in appearance from the

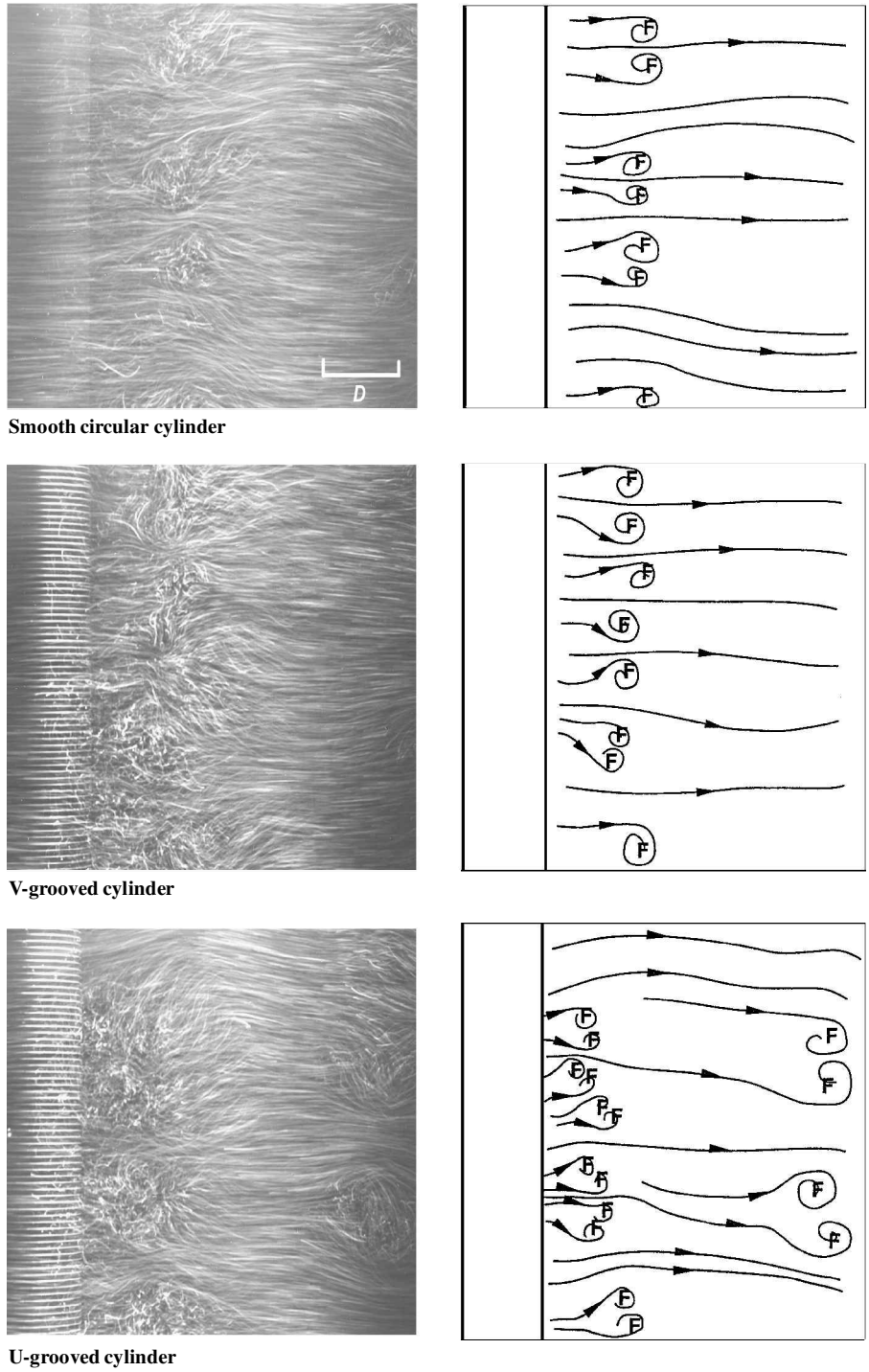

Smooth circular cylinder

V-grooved cylinder

U-grooved cylinder

Fig. 14 Flow visualization in horizontal plane.

large-scale, periodic vortices in the main flow. They[31] also reported that the secondary vortices are formed in the shear layer between the freestream and the vortex formation region, moving downstream by the convecting large-scale vortices.

Figure 12 shows the particle streaks in the streamwise vertical plane of the wake for the smooth, V-grooved and U-grooved cylinders at Reynolds number $Re_D = 1.25 \times 10^4$. The general flow pattern of the wake shown in the photographs looks similar for the three types of cylinders. However, detailed observation shows that the length of the vortex formation region increases for the grooved cylinders. In particular, the U-grooved cylinder has larger vortex formation region than that of V-grooved cylinder. This agrees qualitatively with the earlier results including drag coefficient, pressure distribution, and Strouhal number, even though there are some differences in Reynolds numbers. Flow visualization results show that the large-scale vortices formed behind the U-grooved cylinder have elongated more than 50% compared with those for the smooth cylinder.

Flow visualization study with a particle tracer method was carried out for both the vertical and horizontal planes. The instantaneous topological features of the near wake were identified using the critical-point theory[21]. Even though the flowfield is unsteady, the instantaneous streamline patterns show the general flow pattern, momentum transfer of eddies formed behind the cylinders.

Figure 13 represents the visualized flows captured in the spanwise vertical plane, showing the three-dimensional secondary vortices at the downstream location $x/d = 1.0$. On the right-hand side of each visualized flow image, the streamwise secondary vortices estimated using the critical-point theory were presented. These cross-sectional views clearly reveal the lateral vortical structure induced by the three-dimensional deformation of the secondary vortices. In the visualized flows for the smooth and V-grooved cylinders, large and small vortices exist together. However, the vortices formed behind the U-grooved cylinder are more active and the size of vortices on average is smaller compared with the other two cases. This seems to be attributed to that the secondary vortices behind the U-grooved cylinder are suppressed and broken into smaller eddies due to sharp peaks of the longitudinal U-shaped grooves. These results are in good agreement with the nondimensional PSD results in which the cylinder having a grooved surface has higher shedding frequency than the others.

Figure 14 shows the flowfield visualized in the horizontal plane using the particle tracer method. It shows the top view of longitudinal secondary vortices formed behind the cylinders. However, the longitudinal vortices formed behind the grooved cylinders show rapid motion along the spanwise direction and are more active than those of the smooth cylinder. The secondary vortices behind the U-grooved cylinder are located much closer to the cylinder compared with the other two cases.

From these results, we can see that the longitudinal-grooved surface modifies largely the flow structure near the cylinder, causing a boundary-layer transition and controlling the vortical structure in the near wake.

Conclusions

The flow characteristics of the wake behind circular cylinders with different groove configurations (U and V shape) have been investigated experimentally. The drag force, wake velocity, and surface pressure distribution were measured for Reynolds numbers in the range $Re_D = 8 \times 10^3 \sim 1.4 \times 10^5$. The results are summarized as follows:

1) The U-grooved cylinder was found to reduce the drag coefficient by up to 18.6% compared with the smooth cylinder at $Re_D = 1.4 \times 10^5$, whereas the reduction for the V-grooved cylinder was only 2.5%. The drag reduction of the U-grooved cylinder increased with increasing Reynolds number.

2) With increasing Reynolds number, the length of the vortex formation region and Strouhal number for the U-grooved cylinder increase compared with the smooth and V-grooved cylinders.

3) For U-grooved cylinder, the deficit of mean velocity in the near wake is smaller than that for the smooth cylinder. The U grooves on the cylinder decrease the turbulence intensity in the near wake and shift the maximum point downstream along the wake centerline.

4) Compared with the smooth and V-grooved cylinders, the pressure distribution on the U-grooved cylinder shows large variation around the separation region of the cylinder. As the Reynolds number increases, the separation point shifted downstream, and the surface pressure is decreased.

5) Flow visualization results show that the U-grooved cylinder elongates the vortex formation region more than 50%, compared with the smooth cylinder. Particle streaks visualized in the horizontal plane show a nearly straight pathline for the smooth cylinder. For the U-grooved cylinder, active longitudinal vortices are formed near the cylinder, compared with the other two cases.

6) The vortical structure formed behind the smooth cylinder and V-grooved cylinder consists of large and small secondary vortices in the spanwise vertical plane, whereas the secondary vortices behind the U-grooved cylinder are suppressed and broken into smaller eddies due to sharp peaks of the U-grooved cylinder surface.

Acknowledgment

This work was supported by the National Research Laboratory, sponsored by Ministry of Science and Technology of the Republic of Korea.

References

[1]Gad-el-Hak, M., "Flow Control," *Applied Mechanics Reviews*, Vol. 42, No. 10, 1989, pp. 261–293.

[2]Bandyopadhyay, P. R., "Review—Mean Flow in Turbulent Boundary Layers Disturbed to Alter Skin Friction," *Journal of Fluids Engineering*, Vol. 108, June 1986, pp. 127–140.

[3]Walsh, M. J., "Riblets as a Viscous Drag Reduction Technique," *AIAA Journal*, Vol. 21, No. 4, 1983, pp. 485, 486.

[4]Bacher, E. V., and Smith, C. R., "Combined Visualization–Anemometry Study of the Turbulent Drag Reducing Mechanisms of Triangular Microgroove Surface Modifications," AIAA Paper 85-0546, 1985.

[5]Bechert, D. W., and Bartenwerfer, M., "The Viscous Flow on Surfaces with Longitudinal Ribs," *Journal of Fluid Mechanics*, Vol. 206, 1989, pp. 105–129.

[6]Choi, K. S., "Near-Wall Structure of a Turbulent Boundary Layer with Riblets," *Journal of Fluid Mechanics*, Vol. 208, 1989, pp. 417–458.

[7]Williamson, C. H. K., "Vortex Dynamics in the Cylinder Wake," *Annual Review of Fluid Mechanics*, Vol. 28, 1996, pp. 477–539.

[8]Zdravkovich, M. M., "Review and Classification of Various Aerodynamics and Hydrodynamic Means for Suppressing Vortex Shedding," *Journal of Wind Engineering and Industrial Aerodynamics*, Vol. 7, 1981, pp. 145–189.

[9]Weaver, W., "Wind-Induced Vibration in Antenna Members," *Journal of Engineering Mechanics Division*, Vol. 87, Feb. 1961, pp. 141–165.

[10]Nebres, J. V., and Batill, S. M., "Flow About Cylinders with Helical Surface Protrusions," AIAA Paper 92-0540, 1992.

[11]Lee, S. J., and Kim, H. B., "The Effect of Surface Protrusions on the Near Wake of a Circular Cylinder," *Journal of Wind Engineering and Industrial Aerodynamics*, Vol. 69, No. 10, 1997, pp. 351–361.

[12]Lee, S. J., and Lee, S. H., "Flow Field Analysis of Turbulent Boundary Layer over a Riblet Surface," *Experiments in Fluids*, Vol. 30, No. 2, 2001, pp. 231–246.

[13]Achenbach, E., "Influence of Surface Roughness on the Crossflow Around a Circular Cylinder," *Journal of Fluid Mechanics*, Vol. 46, 1971, pp. 321–335.

[14]Guven, O., Farell, C., and Patel, V. C., "Surface Roughness Effects on the Mean Flow Past Circular Cylinders," *Journal of Fluid Mechanics*, Vol. 98, 1980, pp. 673–701.

[15]Ko, N. W. M., Leung, Y. C., and Chen, J. J. J., "Flow past V-Groove Circular Cylinder," *AIAA Journal*, Vol. 25, No. 6, 1987, pp. 806–811.

[16]Leung, Y. C., and Ko, N. W. M., "Near Wall Characteristics of Flow over Grooved Circular Cylinder," *Experiments in Fluids*, Vol. 10, No. 6, 1991, pp. 322–332.

[17]Gerrard, J. H., "A Disturbance-Sensitive Reynolds Number Range of the Flow Past a Circular Cylinder," *Journal of Fluid Mechanics*, Vol. 22, 1954, pp. 187–196.

[18]Graham, J. M. R., "The Effect of End-Plates on the Two-Dimensionality of a Vortex Wake," *Aeronautical Quarterly*, Vol. 20, No. 3, 1969, pp. 237–247.

[19]Allen, H. J., and Vincenti, W. G., "Wall Interference in a Two-Dimensional Flow and Wind Tunnel with Consideration of the Effect of Compressibility," National Advisory Committee for Aeronautics, Rept. 782, Washington, DC, 1944.

[20]Stansby, P. K., "The Effect of Endplates on the Base Pressure Coefficient of a Circular Cylinder," *Aeronautical Journal*, Vol. 78, Jan. 1974, pp. 36, 37.

[21]Perry, A. E., and Chong, M. S., "A Description of Eddying Motions and Flow Patterns Using Critical-Point Concepts," *Annual Review of Fluid Mechanics*, Vol. 19, 1987, pp. 125–155.

[22]Coleman, H. W., *Experimentation and Uncertainty Analysis for Engineers*, Wiley, New York, 1989.

[23]Wieselsberger, C., "Neuere Feststellungen Uber die Gesetze des Flussigkeits–und Luftwiderstands," *Physikalische Zeitschrift*, Vol. 22, 1923, pp. 321–328.

[24]von Kármán, T., "On Laminar and Turbulent Friction," *Zeitschrift für Angewandte Mathematik und Mechanik*, Vol. 1, 1921, pp. 235, 236.

[25]Bloor, M. S., "The Transition to Turbulence in the Wake of a Circular Cylinder," *Journal of Fluid Mechanics*, Vol. 19, 1963, pp. 290–304.

[26]Roshko, A., "On the Development of Turbulent Wakes from Vortex Streets." NACA Rept. 1191, 1954.

[27]Fage, A., and Falkner, V. M., "The Flow Around a Circular Cylinder," Aeronautical Research Council, Repts. and Memoranda 1369, London, 1931.

[28]Drescher, H., "Messung der auf Querangestromte Zylinder Ausgeubten Zeitlich Veranderten Drucke," *Zeitschrift für Flugwissenschaften*, Vol. 4, No. 1–2, 1956, p. 17.

[29]Ribner, H. S., and Etkin, B., "Noise Research in Canada," *Proceedings of the 1st International Congress on Aerospace Science*, Pergamon, London, 1959.

[30]Gerrard, J. H., "The Mechanics of the Formation Region of Vortices Behind Bluff Bodies," *Journal of Fluid Mechanics*, Vol. 25, 1966, pp. 401–413.

[31]Wei, T., and Smith, C. R., "Secondary Vortices in the Wake of Circular Cylinders," *Journal of Fluid Mechanics*, Vol. 169, 1986, pp. 513–533.

P. R. Bandyopadhyay
Associate Editor